Materialia 12 (2020) 100754

Contents lists available at ScienceDirect

Materialia

journal homepage: www.elsevier.com/locate/mtla

Full Length Article

Ultrasound freeze-casting of a biomimetic layered microstructure in epoxy-ceramic composite materials to increase strength and hardness

Max Mroz[a], James L. Rosenberg[a], Claire Acevedo[a], Jamie J. Kruzic[b], Bart Raeymaekers[a], Steven E. Naleway[a,*]

[a] Department of Mechanical Engineering, University of Utah, 1495 East 100 South, 1550 MEK, Salt Lake City, Utah 84112, United States
[b] School of Mechanical and Manufacturing Engineering, UNSW Sydney, Ainsworth Building (J17), Sydney NSW 2052, Australia

ARTICLE INFO

Keywords:
Bioinspired
Freeze casting
Ultrasound directed self-assembly
Ultrasound freeze casting
Layered epoxy-ceramic composites

ABSTRACT

Some natural materials, such as the dactyl club of the mantis shrimp, have impressive mechanical properties (e.g. strength) due to their microstructure that consists of periodic layers of high and low density material, which prevent crack propagation. Although such layered structures have the potential to increase the strength of engineered epoxy-ceramic composites relative to their constituents, synthetically replicating this class of layered structures in engineered materials has been challenging to date. To overcome this challenge, ultrasound freeze casting (UFC) was used to manufacture macroscale specimens of epoxy-ceramic composite materials with periodic layers of high and low density that mimic the structure of natural materials. The critical operating parameter of the UFC technique, the ultrasound operating frequency, was related to the resulting hardness, porosity, and flexural strength of the resultant epoxy-ceramic composite materials. Scanning electron microscopy and micro X-ray CT was used to visualize the microstructure of the specimens and connect it to the mechanical properties. The ultrasound operating frequency controlled the spacing of the layers as well as the local hardness of the epoxy-ceramic composite, which increased by up to 18%. The flexural strength of the epoxy-ceramic composite was also related to the ultrasound operating frequency, with a maximum increase of 52%.

1. Introduction

The progress of many industries relies on the continual creation of novel high performance and lightweight materials [1]. For example, the aerospace, automotive, and biomedical industries require such materials for applications ranging from structural components to functional scaffolds for tissue ingrowth [2]. Highly porous materials are well suited to the needs of these industries because of their high strength-to-weight ratios. Porous ceramic and epoxy-ceramic composite materials, in particular, are utilized due to their high hardness, strength, and biocompatibility; however, they are often brittle, prohibiting their use in applications that require resilience and toughness [3–6]. The need to overcome these limitations has led many researchers to look to the natural world where composites consisting of brittle mineralized tissue and elastic biopolymers exhibit mechanical strength and toughness that dramatically exceeds the properties of a simple mixture of these constituents [7]. These feats are attributed to sophisticated, hierarchical structures that occur across multiple length scales [1,2,4,7–9]. Synthetically replicating the structures of natural materials with the intent of mimicking their properties has led to a number of engineering breakthroughs in a field known as biomimicry or bioinspired material design [10]. The ubiquity of microstructures observed in natural materials has led to their categorization based on common organizational elements [8]. One such category of structure observed in natural materials is layered structures, or the periodic alternating of regions of different structure and composition [8,11–14]. These layered structures on the microscale result in several different strengthening mechanisms imparting strength and hardness on the macroscale [8,11,13–15]. Replicating the layered microstructure found in natural materials in epoxy-ceramic composite materials has the potential to enhance their mechanical properties. The fabrication of a periodic layered microstructure in epoxy-ceramic composite materials is challenging because it requires assembly of anisotropic features across multiple length scales [1,3,16]. While layered ceramics have demonstrated increased strength and toughness, previous structures have been composed of only dense ceramics, unlike the porous composites found in natural materials [3–5]. These layered composites rely on manufacturing techniques such as stacking ceramic sheets, sequential slip casting, or electrophoretic dispersion which limit the ceramic constituents that can be used and result in heavy, dense materials [3]. To replicate the strength-to-weight ratio, hardness, and strength of natural materials in epoxy-ceramic composite materials, it is necessary to develop a manufacturing technique that creates macroscale composite material samples with alternating layers of different composition and structure on the microscale. In this work, a manufacturing process for porous ceramics,

* Corresponding author.
E-mail address: steven.naleway@mech.utah.edu (S.E. Naleway).

https://doi.org/10.1016/j.mtla.2020.100754
Received 13 February 2020; Accepted 25 May 2020
Available online 3 June 2020

freeze casting, was combined with ultrasound directed self-assembly to create epoxy-ceramic composites with alternating layers of porous and dense ceramics, mimicking the microstructure of natural materials. The ultrasound freeze casting process, and the effect of its process parameters on the material properties of the resulting epoxy-ceramic composites, was characterized.

Freeze casting, or ice templating, is a manufacturing technique that can create 3D biomimetic scaffolds whose porous microstructure is similar to those found in natural materials [6,9,17–22]. However, freeze casting does not allow for anisotropic structural control across length scales, limiting the similarity of freeze-cast scaffolds to natural materials [17]. Freeze casting is a four-step process [17]. (1) A colloid slurry of particles is dispersed in a freezing agent, typically comprising water and polymer binders. (2) The colloid slurry is directionally frozen, such that the growth of ice crystals segregates particles into the interstitial spaces of the dendrites. (3) The freezing agent is removed by sublimation in a freeze drier. (4) The resulting green body is densified via sintering resulting in a complete freeze-cast scaffold. These four steps can be supplemented with a fifth post-processing step such as epoxy infiltration into the pores of the sintered material, which creates an epoxy-ceramic composite material. Freeze casting has been intensively researched due to the variety of materials that can be implemented, such as ceramics [18,23], polymers [24], and composites [6,24]. The process is also simple, inexpensive, scalable [6,9,17–22], and the structure of freeze-cast scaffolds can be controlled through a variety of techniques that can be considered either intrinsic or extrinsic [17].

Intrinsic control includes alterations to the composition of freeze cast slurries, which can be used to increase lamellar wall thickness and affect porosity [1,9,20]. However, control is limited to changes in pore area and pore geometry throughout scaffolds rather than creating a layered structure [9,17,20–22]. The use of large solid loading particles, i.e., alumina platelets, has been demonstrated to closely replicate the structure of the mineral phase of abalone shells [4]. This technique utilized the growth of ice crystals to orient the major axis of high aspect ratio platelets in the direction of freezing, creating a brick structure, but not periodic layers [4]. Extrinsic methods of control are capable of creating site-specific changes to freeze-cast scaffolds and include mechanical templates and external force fields that affect scaffold porosity and microstructure [21,25–29]. Electric fields have been utilized to create dense/porous bilayer ceramic scaffolds [28]. However, this method is incapable of creating more than two distinct regions, and changes in structure were only qualitatively described [28]. The application of a large electrical field (30–150 kV/m) during freezing can alter the preferential orientation of ice crystal growth, i.e., crystals will grow in the direction of an applied electrical field [29]. However, electric fields have not been demonstrated to create layers of unique composition and structure in freeze cast scaffolds [28,29]. Magnetic fields have been used to align particles in a freeze cast scaffold and alter the orientation of the major pore axis [25–27,29]. Methods have relied on permanent magnets to create continuous alterations in pore orientation, rather than discrete layers [25, 26]. Recent research has shown that small uniform magnetic fields (7.8 mT in field strength) can create discrete regions of pore orientation. However, the alterations to pore area and porosity do not mimic the characteristic changes in material composition and structure found in natural materials [17,27,30,31]. Despite the higher degree of user control than with intrinsic methods, extrinsic methods such as magnetic and electrical field-assisted freeze casting are not capable of creating a layered microstructure in freeze-cast scaffolds and limit the constituent materials that can be used [17,21,25–29].

One manufacturing technique capable of extrinsic control of particle suspensions is ultrasound directed self-assembly (UDSA), which enables the manipulation of particles in a fluid medium by means of the radiation force associated with a standing ultrasound wave field [32,33,33]. Specifically, the radiation force drives particles to the nodes of the standing ultrasound wave field. As such, UDSA overcomes the limitations of electrical and magnetic control techniques because it does not require coupling with the external field, and thus works independent of the particle material. Furthermore, this process is scalable due to low attenuation of the ultrasound wave field in low-viscosity fluids [32,33]. UDSA has been applied to freeze casting using a cylindrical transducer during the solidification step of freeze casting to create biomimetic rings of varying porosity across the diameter of scaffolds in a process known as ultrasound freeze casting (UFC) [6]. This work replicated, both in structure and mechanical properties (i.e., hardness), periodic ring structures found in trees and sedimentary rock [6,34]. Inspired by such successes, the present work focuses on developing a new application of UFC for manufacturing periodic layered structures similar to those found in other natural materials such as the dactyl club of the mantis shrimp, which is a composite that is capable of withstanding repeated impacts [13].

2. Materials and methods

2.1. Ultrasound freeze-casting fixture

Fig. 1a displays the setup for manufacturing UFC scaffolds, which consisted of five essential components: a function generator, a 45 dB radio frequency (RF) amplifier, a slurry reservoir, a piezoelectric ultrasound transducer, and a copper cold finger that is submerged in a liquid nitrogen reservoir. The function generator (Siglent SDG1025, Siglent Technologies, Solon, OH, USA) drives the ultrasound transducer at user defined frequencies, amplified by the RF amplifier (440LA, ENI, Rochester, NY, USA). The ultrasound transducer was positioned on top of a 25 × 20 × 22 mm^3 ($y \times x \times z$, as defined in Fig. 1) slurry reservoir such that it contacted the colloid slurry (Fig. 1b). The ultrasound transducer operated as a piston source in the z-direction (see diagram in Fig. 1c). The slurry reservoir rested on top of one end of a copper cold finger, the other end of which extended into an insulated bath of liquid nitrogen. A band heater operated by a PID controller ensured that the temperature of the cold finger dropped at 10 °C/min to create a controlled freeze front to solidify the colloid slurry under lamellar ice growth conditions [6]. The ultrasound freeze casting fixture created for this research contained two substantial differences with the fixture used in previous research [6]; a single plate ultrasound transducer was used and the freeze front acted as reflector, thus establishing a standing ultrasound wave, and the geometry of the transducer and the reservoir used were rectangular.

2.2. Ultrasound transducer operating frequencies

UDSA has been performed between parallel plate ultrasound transducers with identical operating parameters to create a standing ultrasound wavefield between their parallel faces [32,35]. However, in this work, a single ultrasound transducer was used. To establish a standing ultrasound wavefield using a single ultrasound transducer, resonant frequencies of the freezing reservoir were calculated and employed as the ultrasound transducer operating frequencies in this work. The ultrasound transducer operating frequencies were determined to establish a standing ultrasound wave in the z-direction of the freezing reservoir (as diagramed in Fig. 1c) as [36]:

$$f = \frac{v}{2}\left(\frac{n}{L_z}^2\right)^{1/2} \quad (1)$$

where f is the ultrasound operating frequency, v is the sound propagation velocity in the colloidal slurry at room temperature, n is the number of nodes of the standing ultrasound wave, and L_Z =16 mm is the height of the slurry reservoir after compensating for amorphous ice growth during the UFC process [28]. Using a pulse-echo measurement [37] the sound propagation velocity in a colloidal slurry with 10 vol% TiO_2 was determined to be v = 1398 m/s. In this work, three piezoelectric ultrasound transducers with operating frequencies of 0.699 MHz, 1.390 MHz, and

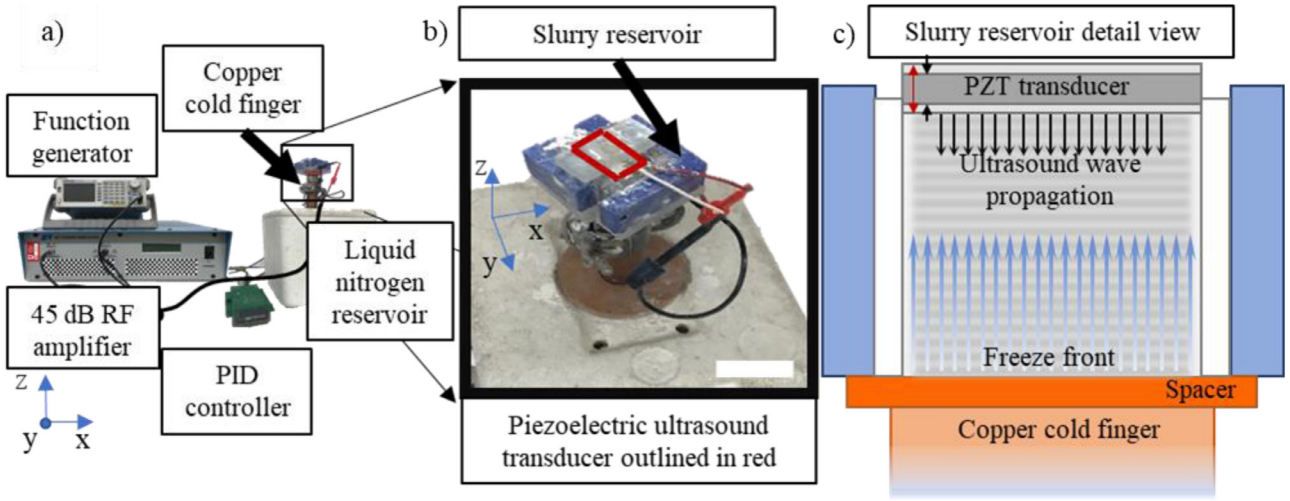

Fig. 1. a) Schematic of the ultrasound freeze casting setup. The PID controller operates a band heater that ensures the temperature of the copper cold finger drops at a rate of 10 ˚C/min. b) A detail view of the slurry reservoir. The piezoelectric transducer is beneath an acrylic backing and covers the colloid slurry. The scale bar is 25 mm. c) A diagram of the ultrasound freeze casting process.

2.097 MHz were used. These ultrasound transducer operating frequencies were selected because they were near the center frequency of commercially available PZT plates that had the same cross-sectional area and were near (± 0.5 MHz) frequencies used in UDSA research [33, 35, 38] and previous UFC research [6]. The transducer operating frequencies that were selected (0.699 MHz, 1.390 MHz, and 2.097 MHz) for this work resulted in a specific number of nodes of the standing ultrasound wavefield, *n* (predicted to be 8, 16, and 24 nodes). Control samples were also produced with a 0 MHz operating frequency.

2.3. Scaffold fabrication

With the exception of the ultrasound operating frequency, all other parameters of scaffold fabrication were kept constant, including the colloid slurry composition, freezing rate, and sintering temperature. Freeze-cast slurries were prepared by combining 10 vol% of TiO_2 particles (< 500 nm diameter, ACROS Organics, Pittsburgh, PA, USA), 1 wt% each of polyethylene glycol (PEG) of 10,000 g/mol (Alfa Aesar, Ward Hill, MA, USA) and polyvinyl alcohol (PVA) of 88,000 – 97,000 g/mol (Alfa Aesar, Ward Hill, MA, USA) as polymeric binders, and 1 wt% Darvan 811 of 3500 g/mol (R.T. Vanderbilt Company, Inc., Norwalk, CT, USA) as a dispersant. 1-Octanol (Sigma-Aldrich, St. Louis, MO, USA) was also added at 0.22 vol% as an antifoaming agent. Ultrasound wavefields show weak attenuation in low viscosity fluids [6,32,35]. The requirement of low viscosity limits slurry constituents such as solidification agents, polymeric binders and the solid loading of the particles, which would raise the slurry viscosity and increase the attenuation of the ultrasound wavefield. Increased wavefield attenuation would require an increase in the field strength to align the particles [32]. In previous freeze casting work, manipulating solidification agents and the solid loading of particles has been demonstrated to affect the kinetics of ice growth, affecting the wall thickness and pore size of freeze cast scaffold structure [17,20]. The constituents of the slurry as well as their respective volume and weight percentages were selected to match previous freeze casting and UFC experimentation to confine changes in the resulting epoxy-ceramic composites to the UFC manufacturing process [6]. These components were mixed with distilled water by ball milling for 16 h with alumina grinding media. After the ball milling was complete, the resultant colloid slurry was frozen in the UFC fixture. The ultrasound transducer was placed onto the top of the slurry reservoir immediately after the it was filled with the colloid slurry and the ultrasound transducer operated throughout the solidification step of UFC.

Seven identical colloid slurries of 60 mL were made, from which one freeze-cast scaffold was frozen at each of the four ultrasound operating frequencies for a total of four freeze-cast scaffolds per slurry. In addition, control freeze-cast scaffolds were manufactured without ultrasound wave field exposure (i.e., 0 MHz). The slurries were frozen at a rate of 10 ˚C/min with the piezoelectric ultrasound transducer operating throughout the entire freezing step, with the exception of the control scaffold that was manufactured without an operating ultrasound transducer. After the freezing step, each freeze-cast scaffold was placed in a freeze drier (Labconco FreeZone 1, Labconco Corporation, Kansas City MO, USA) for 48 h to sublimate the ice. Each freeze-cast scaffold was then densified by sintering in an open-air furnace (Keith KSK-121,700, Keith Company, Pico Rivera CA, USA) at 925 ˚C for 3 h with heating and cooling rates of 2 ˚C/min. After sintering, each freeze-cast scaffold was vacuum infiltrated for 25 min with a two-part potting epoxy (Buehler EpoxiCure 2 resin, Lake Bluff, IL, USA) and allowed to cure for 24 h in ambient air. This process resulted in a total of 28 epoxy-ceramic composites, 7 fabricated with each ultrasound operating frequency: 0 MHz (no ultrasound wave field), 0.699 MHz, 1.390 MHz, and 2.097 MHz. Fig. 2 shows an isometric view of a typical scaffold, indicating a Cartesian coordinate system.

2.3.1. Characterization of scaffold microstructure

To qualitatively characterize the layered microstructure of the epoxy-ceramic composites manufactured with UFC, three-dimensional imaging using helical cone-beam micro X-ray computed tomography (μXCT) was conducted. This provided evidence that the layered microstructure penetrated throughout the entire thickness of the epoxy-ceramic composite materials. Samples of 3 mm in diameter and 5 mm in height were removed from the center of each epoxy-ceramic composite. The μXCT imaging was performed at the Tyree X-ray facilities at the University of New South Wales using a HeliScan^{TM} μXCT. The system has a Hamamatsu X-Ray tube with a diamond window, a high-quality flatbed detector (3072 × 3072 pixel, 3.75 fps readout rate) and a helical scanning system. The samples were scanned in a helical trajectory with the following settings: 80 kV X-ray source, 93 μA target current, 0.43 s exposure time, 4 accumulations, 2520 projections per revolution, and 1 mm Al filter. The voxel size obtained was 1.67 μm. The tomographic reconstruction was performed using QMango software developed by the

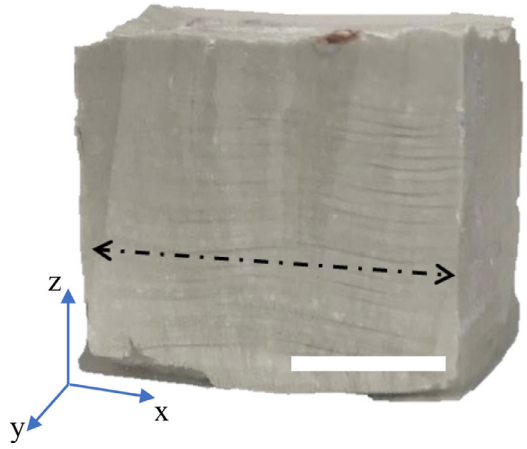

Fig. 2. Isometric view of a typical ultrasound freeze cast epoxy-ceramic composite. The layered microstructure is discernable in the z-direction, with the alternating layers extending in the x-y plane. The dashed arrow points out the layer orientation along the x-direction. The freeze front traveled in the z-direction. The scale bar is 10 mm.

Australian National University. Additional information on helical cone-beam μXCT scanning and reconstruction methods may be found in [39]. Dragonfly 3D software by ORS, Inc. (Montreal, Quebec, Canada) was used to visualize the reconstructed images.

To measure the porosity, periodic feature spacing, and feature length of the layered microstructure, scanning electron microscopy (SEM) images from multiple epoxy-ceramic composites manufactured at the same ultrasound operating frequency were used. A $7 \times 7 \times 7$ mm^3 section removed from each epoxy-ceramic composite, parallel to its x-z plane (see Fig. 3), was imaged using the backscatter detector of an SEM (FEI Quanta 600 FG, Hillsboro, Oregon, USA). From these images, three characteristics of the epoxy-ceramic composite microstructure were determined; (1) the porosity, or percentage of the scaffold that was composed of epoxy, (2) the periodic feature spacing between periodically alternating material layers, and (3) the feature length (Fig. 3c–e). To measure the epoxy-ceramic composite porosity, the SEM images were converted into binary images by thresholding in ImageJ software (National Institute of Health, Bethesda, MD, USA) such that pore areas (that were filled with two-part epoxy) were white and TiO_2 particles black (Fig. 3d). The porosity of the adjacent "dense" and "lamellar" layers resulting from UFC were measured separately, and were characterized by either a lack of pore structure (dense) or a lamellar structure as is typically seen in freeze-cast scaffolds during lamellar ice growth (Fig. 3c). From the 28 epoxy-ceramic composites manufactured, sections were taken from 20 and imaged in 3 randomly selected locations for a total of 60 images. From these images, 45 porosity measurements were collected for each the dense and lamellar region, per ultrasound operating frequency (i.e., 90 per epoxy-ceramic composite with a layered microstructure and 45 per control). To validate the porosity data collected from the SEM images, porosity measurements were also collected from the dense and lamellar regions of the μXCT images. 15 measurements were collected from random locations in both the dense and lamellar layers. The periodic feature spacing and feature length were measured 75 times per ultrasound operating frequency. Previous research has shown that the pore structure of freeze cast scaffolds are susceptible to changes in the thermal gradient that controls the freeze front velocity [17,40,41]. Changes in the thermal gradient and freeze front velocity have been demonstrated to affect the lamellar wall thickness of freeze-cast structures, specifically lower freeze-front velocities lead to thicker lamellar walls [17, 40, 41]. To mitigate the effects of changes in the thermal gradient resulting from the ultrasound transducer operating above the temperature of ambient air, a region of potentially affected material within 5 mm of the top surface of each scaffold was not used for imaging or mechanical testing.

2.3.2. Characterization of scaffold mechanical properties

To measure the hardness within the dense and lamellar regions of each epoxy-ceramic composite, Vickers hardness testing was performed on a cross section parallel to the x-z plane (see Fig. 2), of an epoxy-ceramic composite manufactured with each ultrasound operating frequency, 0 MHz, 0.699 MHz, 1.390 MHz, and 2.097 MHz using a microindenter (LECO M400, LECO Corporation, Saint Joseph, MI, USA). A total of 60 hardness measurements were collected each from the dense and lamellar regions, from an epoxy-ceramic composite manufactured with each ultrasound operating frequency. The Vickers hardness value was calculated as described in [42].

Three-point bend testing was performed following ASTM Standard C1161-18 for flexural strength of advanced ceramics at ambient temperature [43] to calculate the ultimate flexural strength (UFS) and understand the effect of UFC on the macroscopic flexural strength of the epoxy-ceramic composites, using a Psylotech load frame (μTS, Psylotech Incorporated Evanston, IL, USA) with a 220 N load cell at a bending rate of 0.2 mm/min. Three-point bend tests were performed on $21 \times 3.5 \times 2.5$ mm^3 ($x \times y \times z$, see Fig. 2 to interpret the coordinate directions) beams extracted from the center of epoxy-ceramic composites. 10 beams were tested for each of the ultrasound operating frequencies, 0 MHz, 0.699 MHz, 1.390 MHz, and 2.097 MHz for a total of 40 tests. The beam height encompassed 3 dense and lamellar layers for epoxy-ceramic composites manufactured with the lowest ultrasound operating frequency (0.699 MHz) which possessed the largest periodic feature spacing and therefore ensured all the beams tested would possess multiple periodic layers.

2.4. Statistical analysis

The porosity, periodic feature spacing, and feature length data obtained from epoxy-ceramic composite materials manufactured with each ultrasound operating frequency were compared via a one-way ANOVA. Once a statistically significant difference was identified in the data set, a Tukey's HSD test was used to compare each subset of data to determine which groups exhibited a statistically significant difference. All analysis was performed in MATLAB with statistical significance determined by a confidence level of 95%, i.e., a p value smaller than $p = 0.05$ indicated a statistically significant difference. Statistical significance is indicated graphically by non-matching letters in all figures. For the porosity data, the dense and lamellar regions resulting from the UFC process at each ultrasound operating frequency was compared to each other ($N = 45$ measurements each for the dense and lamellar regions per ultrasound operating frequency), as well as to the porosity of the control scaffold ($N = 45$ measurements from SEM images, $N = 15$ from μXCT). A pairwise comparison between each of the ultrasound operating frequencies was performed for the periodic feature spacing measurements ($N = 75$ measurements per ultrasound operating frequency), as well as the feature length measurements ($N = 75$ measurements per ultrasound operating frequency). The mechanical testing data was compared in a similar manner to the microstructure. A pairwise comparison was also performed between the UFS data collected at each ultrasound operating frequency ($N = 10$ measurements per ultrasound operating frequency) and the Vickers Hardness data ($N = 60$ measurements each for the dense and lamellar region, per ultrasound operating frequency).

3. Results and discussion

3.1. Scaffold microstructure

Fig. 4 displays an optical image of a typical control epoxy-ceramic composite and an epoxy-ceramic composite material manufactured with UFC using an ultrasound operating frequency of 1.390 MHz. Fig. 4 also

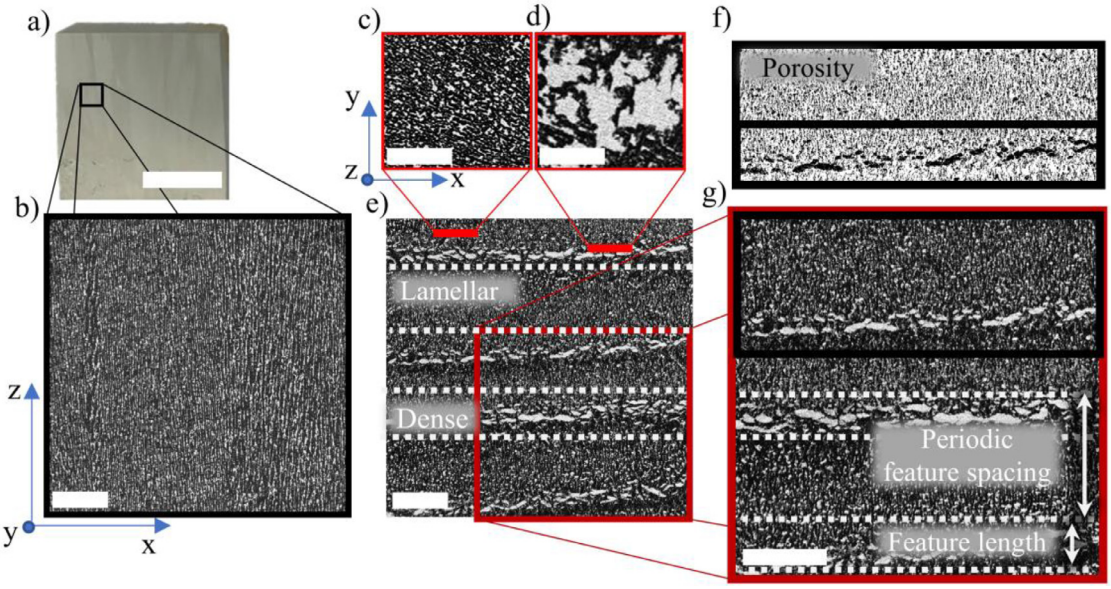

Fig. 3. SEM images of a control and UFC epoxy-ceramic composite cross-section. a) is a typical control scaffold and subsection b) displays an SEM image of the pore structure. c) shows a x-y cross section of the lamellar region and d) is a x-y cross section image of the dense region. e) shows an SEM image of the layered microstructure of a UFC scaffold in the x-z plane with the dense and lamellar regions labeled. f) displays a binarized image with isolated sections to demonstrate the image processing and area that was used to measure porosity. g) provides an example of the location of the periodic feature spacing and feature length measurements. The freezing direction is parallel to the z axis. Scale bars are a) 10 mm b)-g) 500 μm.

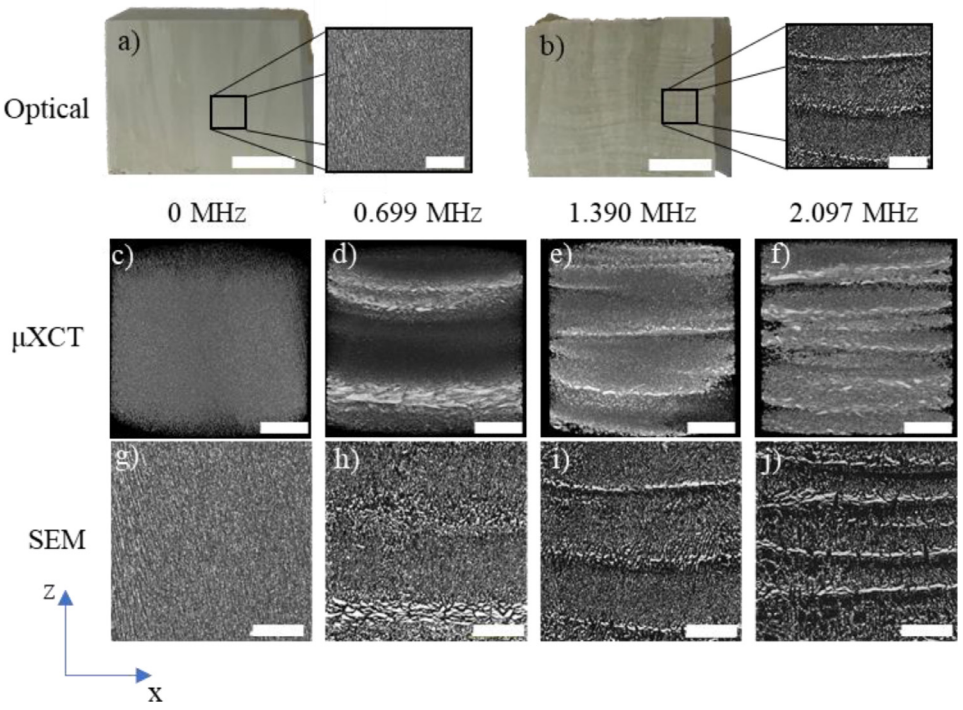

Fig. 4. Images from three imaging techniques; optical, μXCT, and SEM. a) a control epoxy-ceramic composite with no features present and a schematic of the location of the SEM image b) a UFC epoxy-ceramic composite from an ultrasound operating frequency of 1.390 MHz and a schematic of the location of the SEM image c)-f) Micro-CT images of epoxy-ceramic composites with ultrasound operating frequencies of 0 MHz, 0.699 MHz, 1.390 MHz, 2.097 MHz, respectively g)-j) SEM images of epoxy-ceramic composites with ultrasound operating frequencies of 0 MHz, 0.699 MHz, 1.390 MHz, 2.097 MHz, respectively. Scale bars are 10 mm and 500 μm for the optical and SEM images in a) and b), respectively. Scale bars are 200 μm for c)-f), and 100 μm for q)-j).

shows μXCT and SEM images of epoxy-ceramic composites manufactured with each of the four ultrasound operating frequencies. The μXCT scans are presented in grayscale, where a lighter color indicates a denser material (Fig. 4c-4f). While the lamellar region is similar to the structure found in the control, the dense region is different. The contrast between the dense and lamellar regions in the scaffolds indicates an increase in the concentration of the TiO_2 phase in these areas, which is hypothesized to occur due to an increased particle concentration in these regions during freezing because of the radiation force that drives particles to the nodes of the standing ultrasound wave field [38]. The μXCT images provide qualitative evidence of the three-dimensional nature of the periodic layered microstructure present in UFC epoxy-ceramic composites. These images also provide qualitative evidence of the ability of UFC to create epoxy-ceramic composites with a microstructure characterized by layered changes in concentration of constituents. The results of the SEM image processing provide quantitative data on the relationship between ultrasound operating frequency, periodic feature spacing and the feature length.

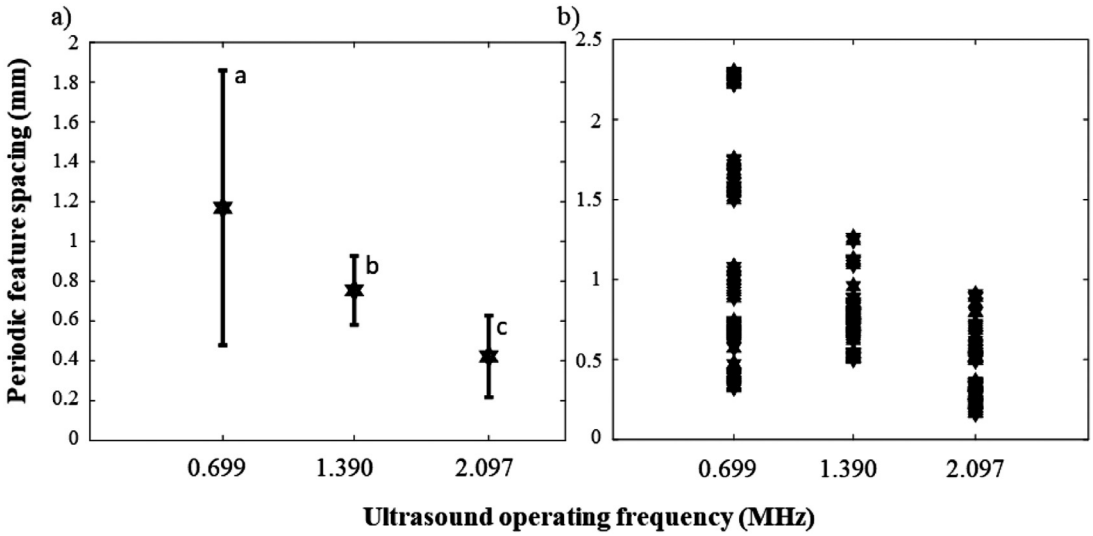

Fig. 5. Plots displaying a) the periodic feature spacing of UFC epoxy-ceramic composites and b) the distribution of the collected measurements. In a) data is presented as the mean with error bars representing ± one standard deviation of $N = 25$ measurements. Statistically significant differences (i.e. $p<0.05$) between length measurements are denoted by non-matching letters. In b) each marker represents an individual measurement.

Fig. 5a displays the periodic feature spacing from the SEM images as a function of the ultrasound operating frequency, to illustrate the effect of the ultrasound operating frequency on the spacing between adjacent dense and lamellar layers. A scatter plot of these measurements is displayed in Fig. 5b. As the ultrasound operating frequency increased, the periodic feature spacing between repeating layers decreased by a statistically significant amount ($p<10^{-6}$). From this decrease in periodic feature spacing, it is clear that the separation of repeating layers in the epoxy-ceramic composite microstructure was a function of the ultrasound operating frequency, as was expected based on UDSA theory [32,38] and previous UFC work [6]. This result is indicative of the ability of UFC to overcome the limitations of previous attempts at creating a layered microstructure in freeze cast epoxy-ceramic composites because the periodic feature spacing is much larger than the pore or particle length [3,4]. The periodic feature spacing and the feature length are determined by the location of the nodes of acoustic pressure and are determined by the operating parameters of the ultrasound transducer [6,32,35]. While it is predicted the periodic feature spacing and feature length are independent of freezing rate, testing this hypothesis was outside the scope of this research.

The feature length of the dense and lamellar features as a function of the ultrasound operating frequency is illustrated in Fig. 6a and a scatter plot of these measurements is presented in Fig. 6b. As was observed in the periodic feature spacing, the length of both regions displayed a decreasing trend as ultrasound operating frequency increased. The decrease in the length of lamellar regions was more significant than the decrease observed in the dense regions, and the length of the lamellar regions produced at each ultrasound operating frequency varied from one another by a statistically significant amount ($p<10^{-4}$). The dense region length produced at 2.097 MHz varied by a statistically significantly amount from the dense regions produced at 0.699 MHz ($p = 0.0119$), but not the dense regions produced at 1.39 MHz ($p = 0.1095$). In UDSA of particles in a fluid medium it is assumed that, given adequate time, the particles are driven directly to the nodes of acoustic pressure with none left in the space between nodes [38]. As a consequence of this assumption, for a constant quantity of particles, the wavelength of the ultrasound operating frequency should only affect the spacing of the nodes of acoustic pressure (and therefore concentrated particles) and not their size. However, the change in length observed between the dense regions produced at 0.699 and 2.097 MHz suggests that the wavelength of the ultrasound wavefield impacts the concentration of the ceramic phase at the nodes of acoustic pressure. At smaller wavelengths, suspended particles are driven into a smaller region resulting in a smaller dense region in the epoxy-ceramic composite. It is surmised that this is due to the intermolecular forces present in colloid suspensions that are absent in UDSA theory, which inhibits particles from being redistributed across larger distances. Particles in colloidal suspensions are suspended by electrostatic forces that overcome attractive Van der Waals forces driving particles towards agglomeration. These forces are on the μN scale (~10–400 μN), and spherical particles < 500 nm in diameter (i.e. the size of the TiO_2 particles used in this research) result in interparticle pressures on the order of 1 GPa [44–46]. However, these forces decay to zero rapidly with interparticle distance and only reach this magnitude when interparticle spacing decreases to less than ~30 nm [46]. In previous UDSA work, the pressure resulting from ultrasound wavefields generated in fluids by piezoelectric transducers operating at similar frequencies was measured to be between 50–60 kPa [47]. For particles separated by even small distances (i.e. greater than 30 nm) the acoustic pressure in the fluid at the nodes of acoustic pressure is adequate to overcome dispersion forces. The pressure exerted by the acoustic radiation force on a spherical particle suspended in a fluid has also been demonstrated to highly depend on frequency (i.e. at particular frequencies the acoustic pressure is higher) [48–51]. The frequency-pressure relationships are highly dependent upon properties of the spherical particle and are not linear [48,49]. Based on the size and porosity of the dense regions at the highest transducer operating frequency it is hypothesized this operating frequency results in a larger acoustic radiation force on TiO_2 particles. However, experimental research into the effect of frequency on the accuracy of the UDSA process does not yet exist in the literature [35]. Evidence that higher transducer operating frequencies lead to a higher concentration of particles at the nodes of acoustic pressure can also be found in Fig. 5b and Fig. 6b where measurements of periodic feature spacing and feature length are less scattered around the mean value at higher frequencies.

The results of the porosity measurements as a function of the ultrasound operating frequency are shown in Fig. 7. The porosity was calculated as the percentage of the imaged area that was composed of epoxy. The two layered regions visible in UFC epoxy-ceramic composites were quantitatively distinguished by their porosity, with the dense regions (red diamonds) displaying lower porosities than the lamellar regions (black stars). The control epoxy-ceramic composite (blue rectangle) showed no distinct regions. There were statistically significant

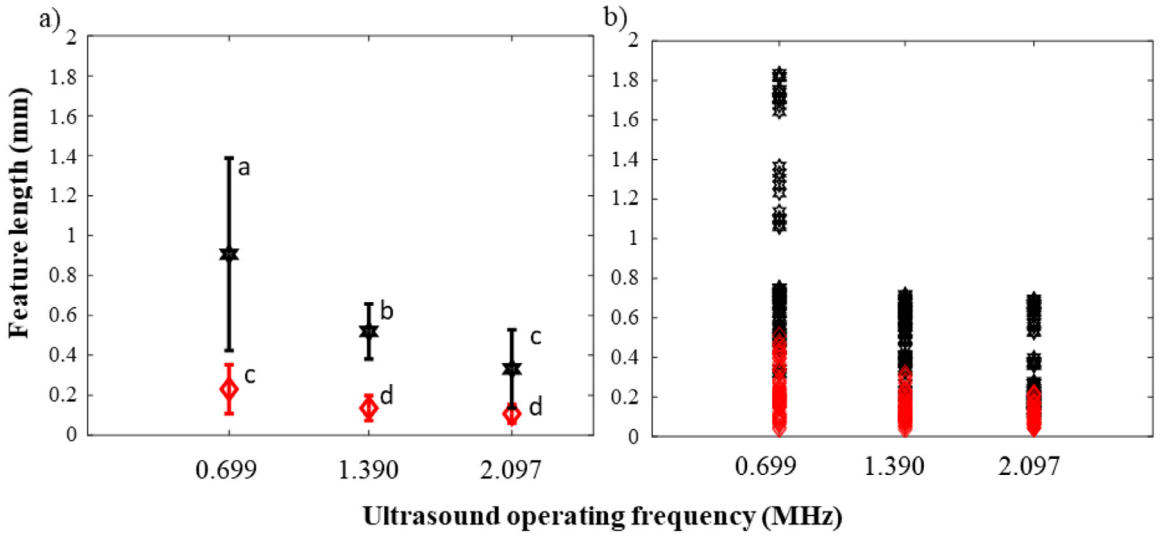

Fig. 6. Plots displaying a) the feature length of UFC epoxy-ceramic composites and b) the distribution of the collected measurements. In both figures the black stars represent the lamellar regions and the red diamonds represent the dense regions. In a) data is presented as the mean with error bars representing ± one standard deviation of $N = 25$ measurements. Statistically significant differences (i.e. $p<0.05$) are denoted by non-matching letters. In b) each marker represents an individual measurement.

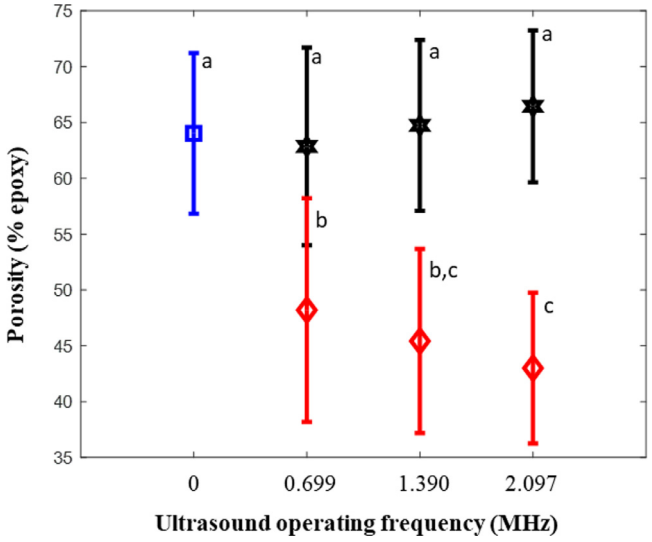

Fig. 7. Plot displaying the porosity of UFC epoxy-ceramic composites. The red diamonds indicate measurements taken in the dense scaffold regions, the black stars represent measurements of the lamellar regions, and the blue square represents the control. Data is presented as the mean with error bars representing ± one standard deviation. Each point represents $N = 45$ measurements and statistically significant differences (i.e. $p<0.05$) are represented by non-matching letters.

differences ($p < 10^{-6}$) in porosity between the control and the dense regions of epoxy-ceramic composites frozen at all three ultrasound operating frequencies. The dense regions also displayed statistically significant differences from the lamellar regions ($p<10^{-6}$) produced at the same ultrasound transducer operating frequency. The porosity measurements collected from the μXCT images did not show a statistically significant difference from the porosity measurements collected from the SEM images ($p>0.05$). The changes in the local porosity did not result in statistically significant ($p>0.05$) changes in the density of the epoxy-ceramic composite materials on macroscale. The mean ± one standard deviation of the macroscale density was $1.506 \times 10^3 \pm 0.0622 \times 10^3$ kg/m^3, $1.434 \times 10^3 \pm 0.0535 \times 10^3$ kg/m^3, $1.497 \times 10^3 \pm 0.0165 \times 10^3$ kg/m^3, and $1.483 \times 10^3 \pm 0.077 \times 10^3$ kg/m^3 for epoxy-ceramic composites produced at 0, 0.699, 1.390, and 2.097 MHz, respectively. The UFC epoxy-ceramic composites displayed layered structures that were distinguishable by differences in the concentration of the ceramic and epoxy phases, rather than regions of differing ceramic phase [3]. None of the lamellar regions displayed statistically significant differences ($p_{avg} = 0.7982$) from the control epoxy-ceramic composite. This suggests the lamellar regions of each epoxy-ceramic composite represented areas in which the freeze-cast structure exhibited no measurable change in pore structure due to the applied ultrasound wavefield. As discussed earlier, it is hypothesized that these regions remained unaffected by the ultrasound wavefield because the intermolecular forces responsible for particle dispersion in the colloidal slurry [44] were greater than the acoustic radiation force in those regions. This trend matches previous UFC results in which the porous regions of biomimetic rings created with UFC did not demonstrate statistically significant differences in porosity from a control scaffold [6]. The porosity of freeze cast scaffolds is influenced by the kinetics of ice growth [17] and it is understood that changes in particle concentration can affect ice growth and the resulting pore structure (e.g. increase lamellar wall thickness) [17, 41]. However, the lack of pore structure found in the dense regions is unique from structures observed in previous research utilizing particle concentration to create changes in the freeze-cast scaffold structure [17,18,40]. The application of ultrasound during freezing is also understood to induce nucleation of ice crystals at lower degrees of supercooling and enhance convective heat transfer in the fluid [52,53]. The combined effects of induced nucleation and increased convective heat transfer in freeze casting has the potential to increase the velocity of the freeze front, decreasing pore wall thickness [17,54]. The porosity of the dense regions produced at 0.699 MHz and 2.097 MHz varied by a statistically significant amount ($p = 0.0335$). The decrease in porosity indicates a greater concentration of the ceramic phase in the dense regions as the ultrasound operating frequency increased. Pairing this decrease in porosity with the observation of a similar, decreasing trend in the length of the dense regions produced at these two ultrasound operating frequencies suggested that as ultrasound operating frequency increased, particles were driven to smaller, more concentrated nodes.

From the characterization of the periodic feature spacing, feature length, and porosity at four ultrasound operating frequencies, 0 MHz, 0.699 MHz, 1.390 MHz, and 2.097 MHz, three key insights were ap-

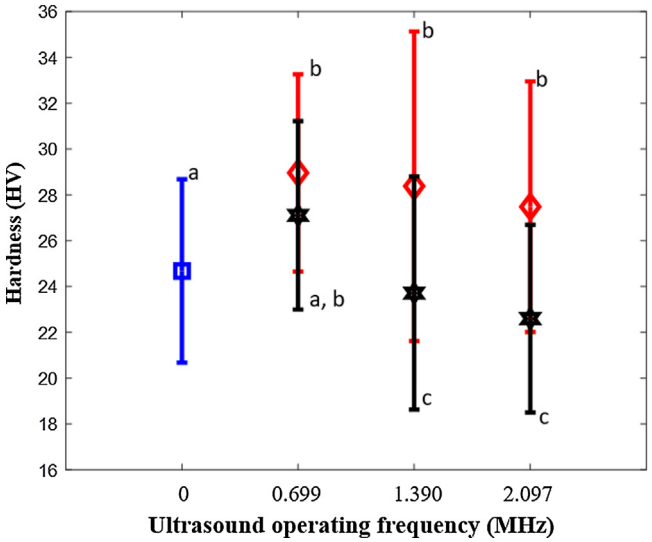

Fig. 8. Plot displaying Vickers Hardness of the two regions within the UFC epoxy-ceramic composites. The lamellar regions are denoted by black stars, the dense regions are denoted by the red diamonds, and the blue square represents the control. Data is presented as the mean with error bars representing ± one standard deviation of $N = 75$ measurements. Statistically significant differences (i.e. $p<0.05$) are represented by non-matching letters.

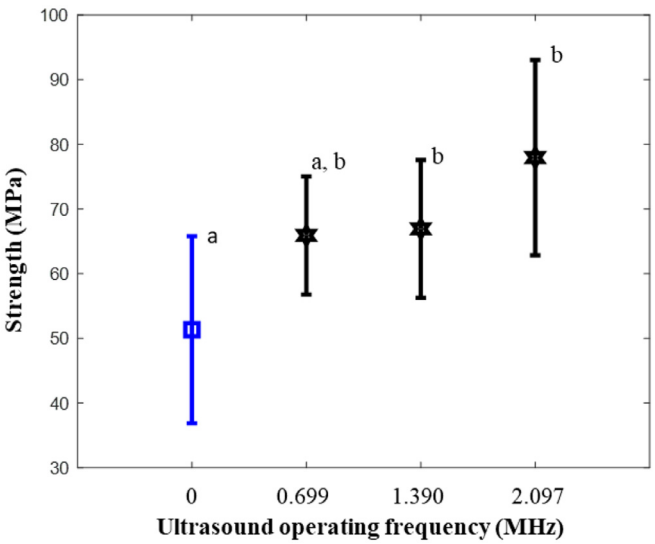

Fig. 9. Flexural strength of UFC epoxy-ceramic composites under 3-point bending. The UFC epoxy-ceramic composites are represented by the black star markers and the control is the blue square. Data is presented as the mean with error bars representing ± one standard deviation of $N = 10$ measurements. Statistically significant differences (i.e. $p<0.05$) are denoted by non-matching letters.

parent. The periodic feature spacing, and therefore the feature concentration (i.e. the number of features in a given cross sectional area), was inversely related to the ultrasound operating frequency. The frequency and number of nodes of acoustic pressure were directly related to one another, but inversely proportional to the wavelength of the resulting ultrasound wavefield [35] that drives the periodic feature spacing. At higher ultrasound transducer operating frequencies, there are more nodes of acoustic pressure separated by a shorter distance. The ultrasound operating frequency affected the location of the dense and lamellar regions as well as their scale. At higher ultrasound operating frequencies, ceramic particles were driven to smaller areas, and they were more concentrated in these regions. From the changes measured in the epoxy-ceramic composite microstructure and their similarity to layered structures found in natural materials, it would be intuitive that UFC epoxy-ceramic composite properties on the macroscale would be affected.

3.2. Scaffold mechanical properties

The collected Vickers hardness measurements as a function of the ultrasound operating frequency are presented in Fig. 8. The dense and lamellar regions are denoted by red diamonds and black stars, respectively. The hardness of the control is marked by a blue square. The dense regions resulting from all three ultrasound operating frequencies were significantly harder than a control epoxy-ceramic composite ($p < 10^{-6}$). The dense regions displayed higher hardness values than the lamellar regions, as was expected based on the difference in porosity discussed earlier, and previous UFC research [6]. When the hardness values were compared between regions resulting from the same ultrasound operating frequency, epoxy-ceramic composites manufactured at 0.699 MHz showed no statistically significant difference in hardness ($p = 0.2417$), though the dense regions did have a higher mean value. The dense and lamellar regions of epoxy-ceramic composites manufactured at 1.390 MHz ($p = 1.68 \times 10^{-7}$) and 2.097 ($p = 6.13 \times 10^{-8}$) MHz did show statistically significant differences in hardness.

The hardness measurements provided another quantitative metric of the differences between regions in the epoxy-ceramic composite's layered microstructure. It is noteworthy that the hardness data shared a common trend with the porosity data described earlier. As the ultrasound operating frequency increased, the p-value of statistical analysis examining the differences between the dense and lamellar regions decreased in both cases, i.e., the difference in properties measured in different regions was larger at higher ultrasound operating frequencies. In the hardness measurements, this decrease in p-value is attributed to the decrease in hardness of the lamellar regions. The lamellar regions produced at 0.699 MHz vary significantly from those produced at 1.390 MHz and 2.097 MHz ($p<10^{-4}$), where the mean hardness value of the lamellar regions produced at the higher frequencies was lower. When comparing the lamellar regions of epoxy-ceramic composites manufactured at 1.390 MHz and 2.097 MHz, there was no statistically significant difference. As the ultrasound operating frequency increased the lamellar regions exhibited less ceramic phase, and their hardness value decreased. This led to a greater difference in local properties of UFC epoxy-ceramic composites resulting from higher ultrasound operating frequencies. The hardness of the lamellar regions of epoxy-ceramic composites produced at 1.390 MHz and 2.097 MHz was lower than that of the control by a statistically significant difference. This is noteworthy due to the lack of change in porosity observed between the control and the lamellar regions of the epoxy-ceramic composite materials. However, the wall thickness of the ceramic phase has been demonstrated to decrease without affecting the scaffold porosity [17,54]. It is hypothesized that this decrease in wall thickness leads to the measured reduction in microscale hardness of the lamellar regions while the porosity remained unaffected.

The macroscopic ultimate flexural strength (UFS) of the UFC epoxy-ceramic composites as a function of the ultrasound operating frequency is presented in Fig. 9. UFC epoxy-ceramic composites are denoted by black stars and the control is represented by a blue rectangle. Epoxy-ceramic composites fabricated at 0.699 MHz showed no statistically significant difference in strength when compared to a control. It is important to note that the p-value associated with the comparison between these two sets of scaffolds was $p = 0.0634$. Therefore, for a confidence level even slightly lower than 95%, the difference would be significant. Epoxy-ceramic composites fabricated at 1.390, and 2.097 MHz did show statistically significant differences from the control with p-values of 0.0418 and 1.9518×10^{-4}, respectively. When compared to the control, the UFC epoxy-ceramic composites displayed an increase in mean UFS of 22%, 30%, and 52% for ultrasound operating frequencies

of 0.699 MHz, 1.390 MHz, and 2.097 MHz, respectively. The increase in macroscale UFS as the ultrasound operating frequency increased was attributed to anisotropic material properties present on the microscale. Based on the differences in local composition, structure, and hardness, it readily follows that the material properties in the dense and lamellar regions, such as stiffness, would be different. It is understood that the strength of layered natural materials relative to their constituents is the result of anisotropic properties on the microscale which prevent crack propagation [4,13,14,19].

The collected data characterizing the microstructure and material properties of UFC epoxy-ceramic composites lead to three main insights regarding the UFC process. The first insight was that the application of an ultrasound wavefield antiparallel to the direction of freezing (z-direction) during freeze casting created a layered microstructure throughout the bulk of epoxy-ceramic composites. The dense and lamellar regions of this microstructure could be quantitatively distinguished on the microscale by porosity and hardness. This layered microstructure mimicked layered structures found in natural materials whose layers are also distinguishable by composition and structure. The second valuable insight was the measured changes in periodic feature spacing and porosity, which made it clear that the location and properties of the layered microstructure was dictated by the ultrasound operating frequency. The third important fact was that the presence of this layered microstructure on the microscale increased the UFS of UFC on the macroscale and that the UFS increased inversely with periodic feature spacing. These results proved that the periodic layered structuring produced by UFC not only qualitatively mimic structures found in nature but also captures their properties producing epoxy-ceramic composites that are up to 52% stronger in flexure.

4. Conclusion

The process of UFC has been demonstrated to affect the structure of epoxy-ceramic composites on the microscale as well as the material properties on the macroscale in the following ways:

- UFC produced a layered microstructure that was composed of dense and lamellar regions distinguishable by their porosity. The dense regions represented the nodes where ceramic particle were driven by the applied ultrasound wavefield. The porosity of the dense regions decreased as the ultrasound operating frequency increased indicating a decrease in node size at higher manufacturing frequencies. A maximum decrease in porosity of 33% when compared to a control resulted from an ultrasound operating frequency of 2.097 MHz.
- The regions of the layered microstructure, dense and lamellar, were also distinguishable by Vickers hardness. A maximum increase in hardness between the dense and lamellar regions of 18% was observed from an ultrasound operating frequency of 2.097 MHz. The hardness measurements of the two distinct regions of UFC epoxy-ceramic composites showed a greater variance as the ultrasound operating frequency was increased. This greater variance in local hardness is attributed to the sparser lamellar regions resulting from higher ultrasound operating frequencies. This is supported by the porosity measurements, which indicated greater particle concentrations in the dense regions resulting from higher ultrasound operating frequencies. It is hypothesized that this change in the ceramic phase concentration in the lamellar regions was due to a decrease in the path length from an antinode to a node of acoustic pressure, i.e., the more concentrated nodes at higher ultrasound operating frequency decreased the distance a particle traveled to a node reducing its susceptibility to other intermolecular forces.
- UFC epoxy-ceramic composites possessed a higher flexural strength than a control. A maximum increase in flexural strength of 52% was observed when the strength of UFC epoxy-ceramic composites manufactured at 2.097 MHz was compared to a control. The flexural strength increased with ultrasound operating frequency and thus decreasing feature spacing, an observation that was attributed to a greater change in local material properties and composition, as evidenced by hardness and porosity measurements. This phenomenon is also observed in the anisotropic material properties found in natural materials.

Declaration of Competing Interest

The authors declare that they have no known competing financial interests or personal relationships that could have appeared to influence the work reported in this paper

Acknowledgments

This work was supported in part by the National Science Foundation under grant CMMI #1660979. The authors further acknowledge the Tyree X-ray CT Facility, a UNSW network lab funded by the UNSW Research Infrastructure Scheme, for the acquisition of the 3D μXCT images.

References

[1] E. Munch, M.E. Launey, D.H. Alsem, E. Saiz, A.P. Tomsia, R.O. Ritchie, Tough, bio-inspired hybrid materials, Science 322 (5907) (2008) 1516–1520 Dec., doi:10.1126/science.1164865.
[2] M.M. Porter, R. Imperio, M. Wen, M.A. Meyers, J. McKittrick, Bioinspired scaffolds with varying pore architectures and mechanical properties, Adv. Funct. Mater. 24 (14) (2014) 1978–1987 Apr., doi:10.1002/adfm.201302958.
[3] F.D. Minatto, P. Milak, A. De Noni, D. Hotza, O.R.K. Montedo, Multilayered ceramic composites – a review, Adv. Appl. Ceram. 114 (3) (Apr. 2015) 127–138, doi:10.1179/1743676114Y.0000000215.
[4] F. Bouville, E. Maire, S. Meille, B. Van de Moortèle, A.J. Stevenson, S. Deville, Strong, tough and stiff bioinspired ceramics from brittle constituents, Nature Mater 13 (5) (May 2014) 508–514, doi:10.1038/nmat3915.
[5] D. Kovar, M.D. Thouless, J.W. Halloran, Crack deflection and propagation in layered silicon nitride/boron nitride ceramics, J. Am. Ceram. Soc. 81 (4) (Jan. 2005) 1004–1112, doi:10.1111/j.1151-2916.1998.tb02438.x.
[6] T.A. Ogden, M. Prisbrey, I. Nelson, B. Raeymaekers, S.E. Naleway, Ultrasound freeze casting: fabricating bioinspired porous scaffolds through combining freeze casting and ultrasound directed self-assembly, Mater Des 164 (February) (2019) 107561, doi:10.1016/j.matdes.2018.107561.
[7] M. Eder, S. Amini, P. Fratzl, Biological composites complex structures for functional diversity, Science (November) (2018) [Online]. Available: https://science.sciencemag.org/content/362/6414/543 .
[8] S.E. Naleway, M.M. Porter, J. McKittrick, M.A. Meyers, Structural design elements in biological materials: application to bioinspiration, Adv. Mater. 27 (37) (Oct. 2015) 5455–5476, doi:10.1002/adma.201502403.
[9] S. Deville, Freezing as a path to build complex composites, Science 311 (5760) (2006) 515–518, doi:10.1126/science.1120937.
[10] A. Jaggessar, H. Shahali, A. Mathew, P.K.D.V. Yarlagadda, Bio-mimicking nano and micro-structured surface fabrication for antibacterial properties in medical implants, J Nanobiotechnol 15 (1) (Dec. 2017) 64, doi:10.1186/s12951-017-0306-1.
[11] G. Mayer, Rigid biological systems as models for synthetic composites, Science 310 (5751) (Nov. 2005) 1144–1147, doi:10.1126/science.1116994.
[12] A.R. Studart, R. Libanori, R.M. Erb, Functional gradients in biological composites, in: D. Ruiz-Molina, F. Novio, C. Roscini (Eds.), Bio- and Bioinspired Nanomaterials, Wiley-VCH Verlag GmbH & Co. KGaA, Weinheim, Germany, 2014, pp. 335–368.
[13] J.C. Weaver, et al., The stomatopod dactyl club: a formidable damage-tolerant biological hammer, Science 336 (6086) (Jun. 2012) 1275–1280, doi:10.1126/science.1218764.
[14] H. Gopalan, A.H. Chokshi, The mechanical behavior of nacre across length scales, J Mech Behav Biomed Mater 78 (Februray) (2018) 96–107, doi:10.1016/j.jmbbm.2017.10.018.
[15] J.W.C. Dunlop, P. Fratzl, Biological Composites, Annu. Rev. Mater. Res. 40 (1) (2010) 1–24 Jun., doi:10.1146/annurev-matsci-070909-104421.
[16] P. Chen, et al., Structure and mechanical properties of selected biological materials, J. Mech. Behav. Biomed. Mater 1 (3) (2008) 208–226 Jul., doi:10.1016/j.jmbbm.2008.02.003.
[17] I. Nelson, S.E. Naleway, Intrinsic and extrinsic control of freeze casting, J. Mater. Res. Technol. (2019) Jan., doi:10.1016/j.jmrt.2018.11.011.
[18] S. Deville, E. Saiz, A.P. Tomsia, Ice-templated porous alumina structures, Acta Mater 55 (6) (2007) 1965–1974 Apr., doi:10.1016/j.actamat.2006.11.003.
[19] S. Deville, Freeze-casting of porous biomaterials: structure, properties and opportunities, Materials 3 (3) (2010) 1913–1927 Mar., doi:10.3390/ma3031913.
[20] S.E. Naleway, et al., Bioinspired composites from freeze casting with clathrate hydrates, Mater Des 71 (2015) 62–67 Apr., doi:10.1016/j.matdes.2015.01.010.
[21] E. Munch, E. Saiz, A.P. Tomsia, S. Deville, Architectural control of freeze-cast ceramics through additives and templating, J. Am. Ceram. Soc. 92 (7) (2009) 1534–1539 Jul., doi:10.1111/j.1551-2916.2009.03087.x.

[22] K.L. Scotti, D.C. Dunand, Freeze casting – A review of processing, microstructure and properties via the open data repository, FreezeCasting.net, Prog Mater Sci 94 (2018) 243–305 May, doi:10.1016/j.pmatsci.2018.01.001.
[23] H.-.L. Hu, Y.-.P. Zeng, Y.-.F. Xia, D.-.X. Yao, K.-.H. Zuo, High-strength porous Si 3N 4 ceramics prepared by freeze casting and silicon powder nitridation process, Mater Lett 133 (2014) 285–288 Oct., doi:10.1016/j.matlet.2014.06.176.
[24] C. Rogers, D. Pun, Q. Fu, H. Zhang, Fabricating MOF/Polymer composites via freeze casting for water remediation, Ceramics 1 (2) (2018) 353–363 Nov., doi:10.3390/ceramics1020028.
[25] M.M. Porter, et al., Magnetic freeze casting inspired by nature, Mater. Sci. Eng. 556 (2012) 741–750 Oct., doi:10.1016/j.msea.2012.07.058.
[26] M.B. Frank, et al., Synergistic structures from magnetic freeze casting with surface magnetized alumina particles and platelets, J. Mech. Behav. Biomed. Mater 76 (2017) 153–163 Dec., doi:10.1016/j.jmbbm.2017.06.002.
[27] I. Nelson, L. Gardner, K. Carlson, S.E. Naleway, Freeze casting of iron oxide subject to a tri-axial nested Helmholtz-coils driven uniform magnetic field for tailored porous scaffolds, Acta Mater. 173 (2019) 106–116 Jul., doi:10.1016/j.actamat.2019.05.003.
[28] Y. Zhang, L. Hu, J. Han, Preparation of a dense/porous bilayered ceramic by applying an electric field during freeze casting, J. Am. Ceram. Soc. 92 (8) (2009) 1874–1876 Aug., doi:10.1111/j.1551-2916.2009.03110.x.
[29] Y. Tang, S. Qiu, Q. Miao, C. Wu, Fabrication of lamellar porous alumina with axisymmetric structure by directional solidification with applied electric and magnetic fields, J. Eur. Ceram. Soc. 36 (5) (2016) 1233–1240 Apr., doi:10.1016/j.jeurceramsoc.2015.12.012.
[30] I. Nelson, et al., Freeze-casting of surface-magnetized iron(ii,iii) oxide particles in a uniform static magnetic field generated by a helmholtz coil, Adv. Eng. Mater. 21 (3) (2019) 1801092 Mar., doi:10.1002/adem.201801092.
[31] I. Nelson, et al., Helical and bouligand porous scaffolds fabricated by dynamic low strength magnetic field freeze casting, JOM (2020) Jan., doi:10.1007/s11837-019-04002-9.
[32] M. Prisbrey, J. Greenhall, F. Guevara Vasquez, B. Raeymaekers, Ultrasound directed self-assembly of three-dimensional user-specified patterns of particles in a fluid medium, J Appl Phys 121 (1) (2017) 014302 Jan., doi:10.1063/1.4973190.
[33] M. Prisbrey, B. Raeymaekers, Ultrasound noncontact particle manipulation of three-dimensional dynamic user-specified patterns of particles in air, Phys. Rev. Appl. 10 (3) (2018) 034066 Sep., doi:10.1103/PhysRevApplied.10.034066.
[34] J. Shahabpour, Liesegang blocks from sandstone beds of the Hojedk Formation, Kerman, Iran, Geomorphology 22 (1) (1998) 93–106 Feb., doi:10.1016/S0169-555X(97)00042-1.
[35] K. Niendorf, B. Raeymaekers, Quantifying macro- and microscale alignment of carbon microfibers in polymer-matrix composite materials fabricated using ultrasound directed self-assembly and 3D-printing, Composites Part A 129 (2020) 105713 Feb., doi:10.1016/j.compositesa.2019.105713.
[36] H. Kuttruff, Acoustics: an Introduction, Taylor & Francis, London; New York, 2007.
[37] M.E. Anderson, G.E. Trahey, The direct estimation of sound speed using pulse–echo ultrasound, J. Acoust. Soc. Am. 104 (5) (1998) 3099–3106 Nov., doi:10.1121/1.423889.
[38] J. Greenhall, F. Guevara Vasquez, B. Raeymaekers, Dynamic behavior of microscale particles controlled by standing bulk acoustic waves, Appl. Phys. Lett. 105 (14) (2014) 144105 Oct., doi:10.1063/1.4898012.
[39] N.A. Yaraghi, et al., A sinusoidally architected helicoidal biocomposite, Adv. Mater. 28 (32) (2016) 6835–6844 Aug., doi:10.1002/adma.201600786.
[40] S. Deville, E. Maire, A. Lasalle, A. Bogner, C. Gauthier, C. Guizard, In Situ X-Ray radiography and tomography observations of the solidification of alumina particles suspensions part I: initial instants, J. Am. Ceram. Soc. 92 (2009) 2489-2496 Oct., doi: 10.1111/j.1551-2916.2009.03163.x.
[41] S. Deville, E. Saiz, A.P. Tomsia, Freeze casting of hydroxyapatite scaffolds for bone tissue engineering, Biomaterials 27 (32) (2006) 5480–5489 Nov., doi:10.1016/j.biomaterials.2006.06.028.
[42] K. Herrmann, Hardness Testing Principles and Applications, ASM international, 2010.
[43] C.2.8. Committee, "Test Method for Flexural Strength of Advanced Ceramics At Ambient Temperature," ASTM International. doi: 10.1520/C1161-18.
[44] D.H. Everett, Chapter 1. What are Colloids? in: RSC Paperbacks, Royal Society of Chemistry, Cambridge, 2007, pp. 1–15.
[45] T. Cosgrove, Charge in colloidal systems, in: Colloid Science: Principles, Methods and Applications, John Wiley & Sons, Inc., 2010, p. 399.
[46] M. Elzbieciak-Wodka, M.N. Popescu, F.J.M. Ruiz-Cabello, G. Trefalt, P. Maroni, M. Borkovec, Measurements of dispersion forces between colloidal latex particles with the atomic force microscope and comparison with Lifshitz theory, J Chem Phys 140 (10) (2014) 104906 Mar., doi:10.1063/1.4867541.
[47] C.R.P. Courtney, C.-.K. Ong, B.W. Drinkwater, A.L. Bernassau, P.D. Wilcox, D.R.S. Cumming, Manipulation of particles in two dimensions using phase controllable ultrasonic standing waves, Proc. R. Soc. A 468 (2138) (2012) 337–360 Feb., doi:10.1098/rspa.2011.0269.
[48] L.W. Anson, R.C. Chivers, Frequency dependence of the acoustic radiation force function (Y p) for spherical targets for a wide range of materials, J. Acoust. Soc. Am. 69 (6) (1981) 1618–1623 Jun., doi:10.1121/1.385938.
[49] T. Hasegawa, T. Kido, C.W. Min, T. Iizuka, C. Matsuoka, Frequency dependence of the acoustic radiation pressure on a solid sphere in water, Acoustical Sci. Technol. 22 (4) (2001) 273–281, doi:10.1250/ast.22.273.
[50] T. Hasegawa, Y. Hino, A. Annou, H. Noda, M. Kato, N. Inoue, Acoustic radiation pressure acting on spherical and cylindrical shells, J. Acoust. Soc. Am. 93 (1) (1993) 154–161 Jan., doi:10.1121/1.405653.
[51] S.R. Aglyamov, A.B. Karpiouk, Y.A. Ilinskii, E.A. Zabolotskaya, S.Y. Emelianov, Motion of a solid sphere in a viscoelastic medium in response to applied acoustic radiation force: theoretical analysis and experimental verification, J. Acoust. Soc. Am. 122 (4) (2007) 1927–1936 Oct., doi:10.1121/1.2774754.
[52] X. Cheng, M. Zhang, B. Adhikari, M.N. Islam, B. Xu, Effect of ultrasound irradiation on some freezing parameters of ultrasound-assisted immersion freezing of strawberries, Int. J. Refrig. 44 (2014) 49–55 Aug., doi:10.1016/j.ijrefrig.2014.04.017.
[53] H. Kiani, D.-.W. Sun, A. Delgado, Z. Zhang, Investigation of the effect of power ultrasound on the nucleation of water during freezing of agar gel samples in tubing vials, Ultrason Sonochem 19 (3) (2012) 576–581 May, doi:10.1016/j.ultsonch.2011.10.009.
[54] P.M. Hunger, A.E. Donius, U.G.K. Wegst, Structure–property-processing correlations in freeze-cast composite scaffolds, Acta Biomater 9 (5) (2013) 6338–6348 May, doi:10.1016/j.actbio.2013.01.012.